THE JOURNAL OF PHYSICAL CHEMISTRY B

ARTICLE

pubs.acs.org/JPCB

Effect of Interfacial Water Transport Resistance on Coupled Proton and Water Transport Across Nafion

May Jean Cheah,[†] Ioannis G. Kevrekidis,[†,‡] and Jay Benziger*[,†]

[†]Department of Chemical and Biological Engineering and [‡]Program in Applied and Computational Mathematics, Princeton University, Princeton, New Jersey 08544, United States

Supporting Information

ABSTRACT: Dynamic and steady-state water flux, current density, and resistance across a Nafion 115 membrane-electrode-assembly (MEA) were measured as functions of temperature, water activity, and applied potential. After step changes in applied potential, the current, MEA resistance, and water flux evolved to new values over 3000−5000 s, indicating a slow redistribution of water in the membrane. Steady-state current density initially increased linearly with increasing potential and then saturated at higher applied potentials. Water flux increases in the direction of current flow resulting from electro-osmotic drag. The coupled transport of water and protons was modeled with an explicit accounting for electro-osmotic drag, water diffusion, and interfacial water transport resistance across the vapor/membrane interface. The model shows that water is dragged inside the membrane by the proton current, but the net water flux into and out of the membrane is controlled by interfacial water transport at the membrane/vapor interface. The coupling of electro-osmotic drag and interfacial water transport redistributes the water in the membrane. Because water entering the membrane is limited by interfacial transport, an increase in current depletes water from the anode side of the membrane, increasing the membrane resistance there, which in turn limits the current. This feedback loop between current density and membrane resistance determines the stable steady-state operation at a fixed applied potential that results in current saturation. We show that interfacial water transport resistance substantially reduces the impact of electro-osmotic drag on polymer electrolyte membrane fuel cell operation.

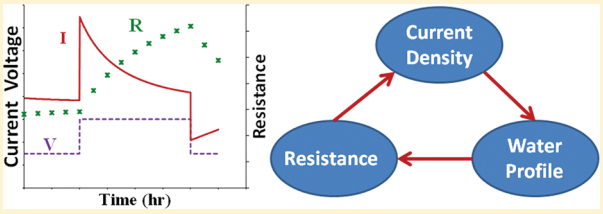

INTRODUCTION

Water management is a major engineering challenge for polymer electrolyte membrane (PEM) fuel cells. Excess water can flood the gas flow channels, hindering mass transport of hydrogen at the anode or oxygen at the cathode, decreasing the fuel cell current. But insufficient water can dehydrate the PEM, increasing the membrane resistance, also decreasing the fuel cell current.

It is widely accepted that electro-osmotic drag (EOD), where the proton current drags water molecules from the anode to the cathode, dehydrates the anode side of the PEM.[1,2] Many EOD studies have claimed that each proton drags one or more water molecules from the anode to the cathode, which would necessitate humidification of the hydrogen feed to PEM fuel cells to ensure that the entire PEM is sufficiently hydrated to conduct the proton current.

However, Nafion PEM fuel cell operation with dry feeds is well documented.[3,4] Commercial units with dead-ended anodes function with no anode humidification and water must even be purged from the anode.[5,6] Hogarth and Benziger showed that operation of Nafion PEM fuel cells with dry feeds (autohumidified operation) could be sustained even at temperatures above 100 °C.[7] Is there an explanation for the apparent contradiction between autohumidified PEM fuel cell operation, and reports that EOD drags one or more water molecules per proton from the anode to the cathode?

A number of papers have been written discussing the mechanism of proton transport and electro-osmotic drag in polymer electrolyte membranes.[8−11] In addition to EOD transport, water is also transported by diffusion across the PEM. Within the PEM, it is usually assumed that the water flux is the sum of water transport by diffusion and by EOD. At the membrane/electrode interface, the proton current stops but water can be transported across the interface. In this paper, we will examine the relationship between the intrinsic electro-osmotic drag of water in a Nafion membrane and the net overall transport of water across a membrane-electrode assembly (MEA).

Inside the membrane, we define the intrinsic EOD coefficient, ξ_m = number of water molecules transported per proton. We define the effective, or *net*, electro-osmotic drag coefficient as the change in water flux across an MEA with current density, $\xi_{net} = F(\mathrm{d}(\text{water flux})/\mathrm{d}(\text{current density}))$, where F is Faraday's constant. We shall show that the two quantities are equal when the membrane/electrode interfacial water transport resistances are negligible. However, when water transport is limited by

Received: May 23, 2011
Revised: July 20, 2011
Published: July 22, 2011

dx.doi.org/10.1021/jp204785t | J. Phys. Chem. B 2011, 115, 10239–10250

Table 1. Summary of EOD Studies

technique (driving force)	source	conditions	electro-osmotic drag coefficient, ξ
activity gradient (chemical potential)	Fuller and Newman, 1992[24]	vapor equilibrated	1.4
		temperature: 25 °C, 37.5 °C	
	Zawodzinski et al., 1995[23]	temperature: 30 °C	
		vapor equilibrated	1.0
		liquid equilibrated	2.5
	Gallagher et al., 2009[25]	vapor equilibrated	~1
		temperature: −25 °C, 10 °C	
electro-osmotic drag cell (applied potential)	Zawodzinski et al., 1993[22]	temperature: 30 °C	
		vapor equilibrated	0.9
		liquid equilibrated	2−2.9
streaming potential (applied pressure)	Xie and Okada, 1995[26]	vapor equilibrated	2.6
		temperature: 25 °C	
electrophoretic NMR (applied potential)	Ise et al., 1999[27]	temperature: 27 °C	1.5−2.5
		vapor equilibrated	
methanol fuel cell (electrochemical)	Ren and Gottesfeld, 2001[28]	liquid equilibrated	
		temperature: 15 °C	2.0
		temperature: 130 °C	5.1
hydrogen fuel cell (electrochemical)	Park and Caton, 2008[29]	vapor equilibrated	0.50−0.82
		temperature: 70 °C	
hydrogen pump (applied potential)	Weng et al., 1996[30]	vapor equilibrated	0.2−0.6
		temperature: 135 to 185 °C	
	Ge et al., 2006[31]	vapor equilibrated	0.2−0.9
		temperature: 30 to 50 °C	
		liquid equilibrated	1.8−2.7
		temperature: 15 to 85 °C	
	Ye and Wang, 2007[32]	vapor equilibrated	1.1
		temperature: 80 °C	
	Luo et al., 2010[33]	liquid equilibrated	2−3.4
		temperature: 20 to 90 °C	
		vapor equilibrated	1.2−2
		temperature: 25 °C	

interfacial transport resistances, the net electro-osmotic drag coefficient is reduced compared to the intrinsic EOD coefficient inside the membrane, i.e., $\xi_{net}/\xi_m \ll 1$.

Over the past 20 years, there have been numerous measurements of EOD in Nafion as a function of temperature (T) and water activity ($a_w = P_w/P_w^\circ$). A review of the various studies on EOD in polymer electrolyte membranes was published in 2006.[12] Table 1 provides an updated summary of the studies on the electro-osmotic drag of protons in Nafion. The literature has not distinguished between the intrinsic EOD coefficient, ξ_m and the net EOD coefficient, ξ_{net}. The majority of the studies reported electro-osmotic drag coefficients, $\xi \geq 1$; we will use ξ unsubscripted where no distinction is made between ξ_m and ξ_{net}.

The values of ξ for Nafion show a large scatter. The most consistent observation is that the reported electro-osmotic drag coefficients are larger when membranes are equilibrated with liquid water and are smaller when membranes are equilibrated with water vapor. Also, for both vapor and liquid equilibrated membranes, the electro-osmotic drag coefficients seem to increase with temperature. It is difficult to compare values of ξ because the environmental conditions are not always fully defined.

We present here experiments and analysis that attempt to distinguish between the intrinsic electro-osmotic drag coefficient (ξ_m) and the net EOD coefficient associated with the overall water flux across the MEA (ξ_{net}). We have paid specific attention

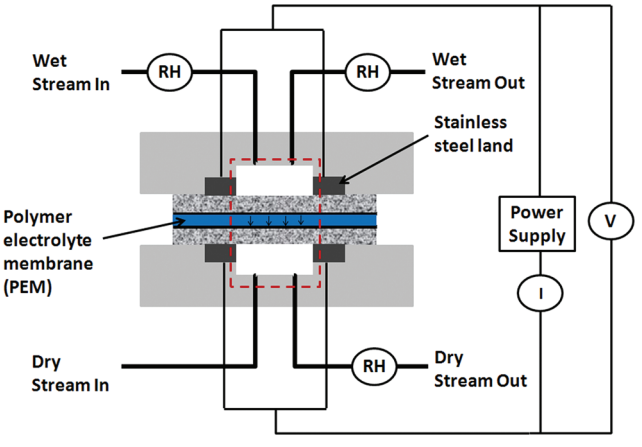

Figure 1. Schematic of the experimental setup. The dotted red box in the figure highlights that due to uniform compositions in both plenums, there is only transverse water transport through the polymer electrolyte membrane (PEM).

to the coupling of interfacial water transport resistance with electro-osmotic drag. This work extends our previous studies of interfacial transport resistances for water transport at the Nafion/vapor interface.[13−15]

The paper is organized as follows: (a) Experimental Methods describe the "one-dimensional" permeation cell used in experiments, where water flux, current, and MEA resistance were measured while water activity, temperature, and applied potential were controlled; (b) Results report the dynamic and steady-state current density, water flux, and MEA resistance measurements; (c) the Discussion analyzes the effects of interfacial transport resistance on the net electro-osmotic drag coefficient, and the water and proton transport processes.

EXPERIMENTAL METHODS

Water flux across the Nafion membrane was measured in the absence and in the presence of a protonic current using a "one-dimensional" permeation cell (Figure 1). Details of the cell fabrication are described elsewhere.[15] A humidified gas stream was supplied to one side of the membrane and a dry gas stream to the other side. The relative humidities of the exiting streams were monitored as a function of time. The water flux was calculated by mass balances. The cell was modified by the addition of stainless steel electrodes to apply an electrical potential across the membrane electrode assembly (MEA). The MEA used in the experiments was made using two silicon gaskets, two carbon cloth gas diffusion layers (GDLs) with a carbon microporous layer on one side (Electrochem Inc., Woburn, MA), and a catalyst coated Nafion 115 membrane (the catalyst coated membrane was purchased from Ion Power Inc., New Castle, DE. The anode and cathode catalyst loadings were listed as 0.3 (mg Pt/cm^2)/side). The surface area of the MEA exposed to the open plenum was 1 cm^2. The MEA was clamped between the plates of the cell and the entire cell assembly was placed inside a temperature-controlled insulated box.

The cell was run in three different flux configurations, defined by the direction of current flow in relation to the external water activity gradient. Hydrogen was supplied to the anode. The applied potential oxidized H_2, and protons flowed from the anode to the cathode. A humidified gas stream was supplied to either the anode or cathode. (i) Co-current flux: Humidified hydrogen was fed to the anode, and dry nitrogen was fed to the cathode. The vapor phase water activity gradient and the current were in the same direction. (ii) Counter-current flux: Dry hydrogen was fed to the anode, and humidified nitrogen was fed to the cathode. The vapor phase water activity gradient and the current were in opposing directions. (iii) No-current: Humidified nitrogen was fed to the "anode", and dry nitrogen was fed to the "cathode".

The water activity of the humidified feed stream was controlled by mixing a water saturated gas stream with a dry gas stream using mass flow controllers. The humidified feed stream was run in large excess to minimize the compositional changes due to current flow. The flow rates of both the humidified feed stream and the dry gas stream were not varied; because of the GDLs, there was a stagnant layer that was not affected by the gas flow rates.

Open plenums on each side of the cell permitted good mixing in the gas phase to ensure that the water vapor activity was spatially uniform in the anode and cathode plenums respectively; this assured that the outlet compositions of the anode and cathode were equal to the compositions inside the plenums. The relative humidity and temperature of the anode and cathode outlets and the humidified feed stream were measured with Sensirion Model SHT75 sensors.

All measurements were taken with the anode and cathode plenums at a total pressure, P_{total}, of 101 kPa. The net water transport across the membrane (i.e., water flux) was equal to the molar water flow exiting the dry side plenum given by eq 1.

$$\text{water flux} = \frac{(\text{RH}/100)P_{\text{W}}^{\circ}(T)}{P_{\text{total}} - (\text{RH}/100)P_{\text{W}}^{\circ}(T)} \frac{P_{\text{std}} Q_{\text{gas, exit}}}{R_{\text{g}} T_{\text{std}}} \text{ mol/s} \quad (1)$$

In eq 1, RH is the measured relative humidity of water, $P_w^{\circ}(T)$ is the saturation pressure of water (kPa) at temperature, T, $P_{standard}$ is the standard pressure (101.325 kPa), $Q_{gas,exit}$ is the volumetric flow rate of the gas stream exiting the dry side plenum (m^3/s), R_g is the ideal gas constant [8.314 × 10^3 (kPa m^3)/(mol K)], and $T_{standard}$ is the standard temperature (298 K).

The water fluxes at the anode and cathode inlets were compared to the water fluxes at the outlets. The overall water mass balances at steady state closed to <5% in all the reported experiments.

Co-current flux experiments were conducted at three different anode feed relative humidities (RH: 30%, 50%, and 70%) and three different temperatures (37, 50 and 70 °C). Additional experiments were done at anode feed RH of 86% and 100%. We were unable to get good quantitative results from the high RH experiments. At high RH, the removal of hydrogen from the anode gas phase as protons were pumped across the PEM caused liquid water to condense, resulting in 20% fluctuations in the overall water balance. Counter-current flux experiments were conducted at 50 °C with a cathode feed RH of 50%. No-current experiments were conducted at 50 °C with "anode" feed RH of 50% and 80%.

The MEA was equilibrated at open circuit for 4−12 h until the relative humidity of the anode and cathode outlets, as well as the MEA's resistance, had equilibrated. After equilibration, an Arbin MSTAT4+ test station was used to apply a sequence of potentials across the cell, where the duration of each applied potential step was 2 h. During each applied potential step, the current and relative humidities of the gas streams were logged by computer every second. The MEA resistance, R_{MEA}, was measured by pulsed current relaxation every 15 min, from the voltage drop after a 4 × 10^{-5} coulomb pulse. The reported R_{MEA} was the average resistance from 10 such pulses.

RESULTS

Dynamic Measurements of Current, Resistance, and Cathode Water Partial Pressure. Figure 2 shows a sample of the dynamic data obtained in a typical co-current flux experimental run. In the first two hours and last two hours of the run, no potential was applied and the observed voltage was the open circuit voltage of the cell due to the difference in hydrogen partial pressure across the MEA. Typical open circuit voltages ranged from 0.1 to 0.15 V. In the experimental run shown, the applied potential, V_{app} was stepped between 0.075, 0.15, 0.3, and 0.6 V in 2 h time intervals. The complete data set for Figure 2 is available as Supporting Information.

Table 2 summarizes the measured initial and steady-state current, i, and MEA resistance (R_{MEA}) values as well as the

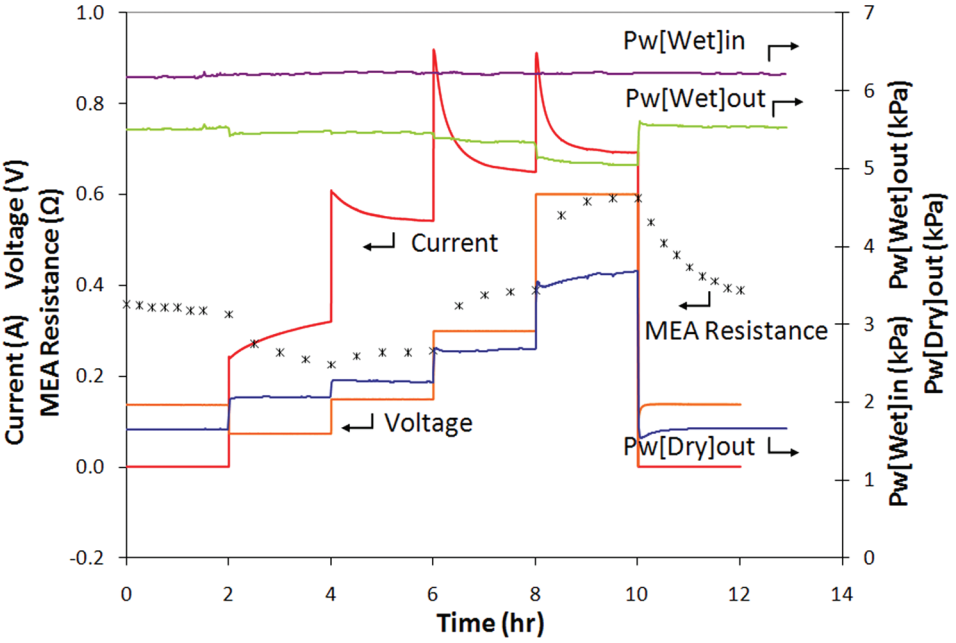

Figure 2. Data set of a typical co-current flux experimental run. This run was conducted with humidified hydrogen (anode feed RH of 50%) and dry nitrogen, at 50 °C. From the second to the 10th hour, the applied potential was stepped from 0.075 to 0.15, 0.3, and 0.6 V in 2 h time intervals.

Table 2. Dynamic Experimental Data at 50 °C, 50% Anode RH

		current (A)		MEA resistance (Ω)		
	applied potential		steady		steady	$p_{w,g}^{cathode}$
time (h)	(V)	initial	state	initial	state	(kPa)
0−2	0	0	0	0.36	0.34	1.65
2−4	0.075	0.24	0.32	0.34	0.23	2.04
4−6	0.15	0.61	0.54	0.23	0.26	2.26
6−8	0.3	0.92	0.65	0.26	0.39	2.69
8−10	0.6	0.9	0.69	0.39	0.59	3.68
10−12	0	0	0	0.59	0.39	1.66

measured cathode water partial pressure, $p_{w,g}^{cathode}$ at each applied potential step based on the experimental data shown in Figure 2.

We highlight four key results in Figure 2 and Table 2 for the reader.

(1) At hour 2, the applied potential was stepped from 0 to 0.075 V and then held at 0.075 V. The resulting current jump was consistent with $\Delta i = \Delta V_{app}/R_{MEA}(@t = 2\ h)$. The relative humidity at the cathode increased. The relative humidity change indicated that there was additional water flux due to electro-osmotic drag.

(2) Between hours 2 and 4, the current increased and R_{MEA} decreased, consistent with Ohm's law $i(t)R_{MEA}(t) = V_{app}$. These transient changes in i and R_{MEA} followed decaying exponentials with a time constant of ~3000 s.

(3) At hour 8, the applied potential was increased from 0.3 to 0.6 V. There was a large immediate current increase consistent with $\Delta i = \Delta V_{app}/R_{MEA}(@t = 8\ h)$. The water flux increased, corresponding to a net electro-osmotic drag coefficient of Δwater flux/Δi = 0.2.

(4) Between hours 8 and 10, the applied potential was held at 0.6 V. The current decreased; the steady-state current decreased almost to the same current obtained at the applied potential of 0.3 V. R_{MEA} increased proportionally to the decrease in current. While the current decreased, the water flux increased; *this would appear to imply a negative electro-osmotic drag!*

The highlighted results suggest that when there is a change in the applied potential, the resulting change in current causes a redistribution of the water in the PEM. The water redistribution takes a long time (>3000 s) and alters the membrane resistance and, in turn, the current. We propose that the water redistribution in the membrane also caused the increase in water flux even as current was decreasing in hours 8−10.

When the cell was returned to open circuit, the current immediately dropped to zero. R_{MEA} decayed exponentially to the initial open circuit R_{MEA} value. The cathode water partial pressure also decayed exponentially to its initial open circuit value.

A total of 45 experimental runs similar to those shown in Figure 2 were conducted with different applied potential profiles, at different temperatures, relative humidities, and flux configurations. At least two data sets were collected at each applied potential for every temperature, feed RH, and flux configuration combination. Experimental runs were obtained with both increasing and decreasing applied potential profile. Data were obtained with several different MEAs, and the results (both water flux measurements and *IV* responses) were highly reproducible for the same experimental conditions. The complete dynamic data sets are available from our Web site (http://pemfc.princeton.edu/EOD_Data).

To reduce the complexity of reviewing all the dynamic data, steady-state results were compiled by taking the limiting values of current, water partial pressures at the anode and cathode, and MEA resistance at the end of each two hour time interval. Water flux was calculated from the cathode water partial pressure using eq 1.

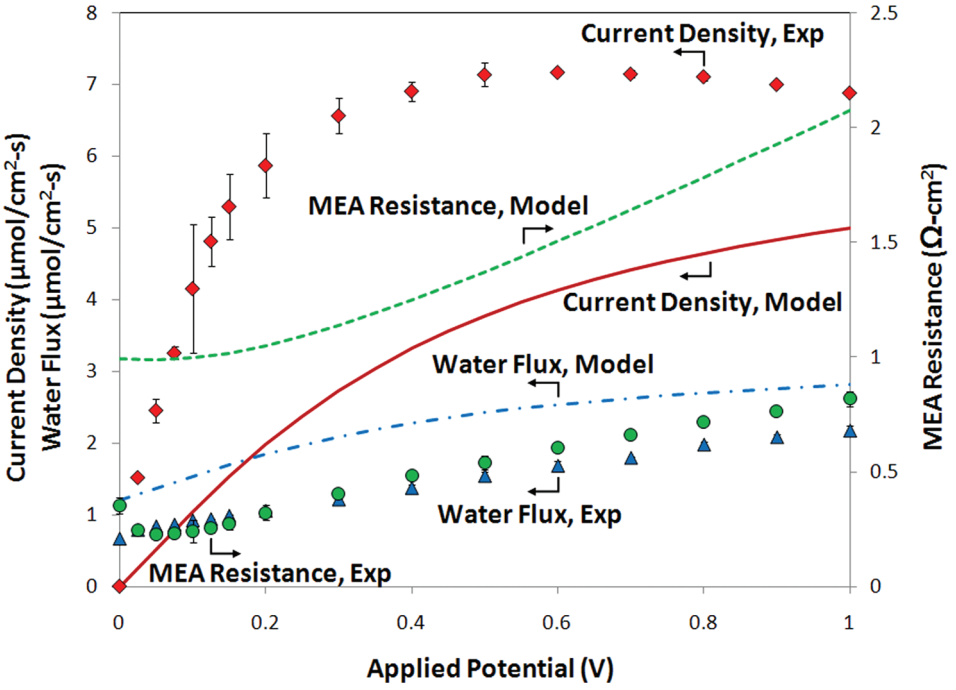

Figure 3. Steady-state current density, water flux, and R_{MEA} as functions of applied potential for co-current flux at 50 °C, 50% RH anode feed. Standard deviations above the marker size are shown: 0.008 A/cm^2 [0.088 μmol/(cm^2 s)] for the current density, 0.017 μmol/(cm^2 s) for the water flux, and 0.01 Ω cm^2 for R_{MEA}. The solid and dashed lines are the results of solving the linear transport model, which will be described in the Discussion. Parameters for the model are listed in Table 4.

Co-current Flux: Current, MEA Resistance, and Water Flux Measurements. Humidified hydrogen was supplied to the anode while dry nitrogen was supplied to the cathode. The measured steady-state open circuit voltages (OCV) of 0.1−0.15 V were due to the difference in hydrogen partial pressure, P_{H_2} across the membrane: $V_H = (R_gT/2F)\ln(P_{H_2}^{anode}/P_{H_2}^{cathode})$, where F is the Faraday constant (96 485 C/mol). Molecular hydrogen diffused through the membrane from the anode to the cathode and was swept away by the nitrogen purge at the cathode. The molecular H_2 diffusion, or crossover flux, is given by eq 2.

$$H_2 \text{ crossover flux} = x_{H_2}^{anode}\frac{P_{std}Q_g^{cathode}}{R_gT_{std}}\exp\left(-\frac{2FV_H}{R_gT}\right) \quad (2)$$

In eq 2, $x_{H_2}^{anode}$ is the mol fraction of hydrogen at the anode. From eq 2, the measured OCV corresponded to hydrogen partial pressures ca. 1 Pa at the cathode and a crossover flux of <1 mA/cm^2. Application of a potential caused a proton current of 100−1000 mA/cm^2 to flow from the anode to the cathode; the proton current was much greater than the crossover flux. Thus, in our analysis, the crossover flux was neglected.

The proton current flow from anode to cathode was co-current to the external vapor phase water partial pressure gradient ($p_{w,g}^{anode} > p_{w,g}^{cathode}$, where $p_{w,g}^{anode}$ and $p_{w,g}^{cathode}$ are the vapor phase water partial pressures at the anode and cathode respectively). Figure 3 shows the steady-state current, R_{MEA}, and water flux as functions of the applied potential for co-current flux at 50 °C and 50% RH anode feed. The most important features in Figure 3 are (i) the current increased at low applied potentials and then saturated at higher applied potentials, (ii) the membrane resistance went through a minimum at an applied potential of ∼0.1 V and then increased with applied potential, and (iii) the water flux increased with applied potential but the water flux increased much less than the current. These features were observed for all co-current flux experiments independent of temperature and relative humidity of the anode feed. Figure 3 also shows the results of solving the linear transport model, which will be described in the Discussion. The entire steady-state data set for Figure 3 and the model calculations are available as Supporting Information.

Figure 4 shows the steady-state current and water flux as functions of applied potential for different anode relative humidities at a temperature of 50 °C. The current increased linearly with increasing applied potential up to about 0.3 V; this will be referred to as the "ohmic regime". For applied potentials, V_{app} > 0.3 V, the current saturated with increasing applied potential; this will be referred to as the "saturation regime". Current saturation at high applied potentials had been observed by other researchers.[16,17]

The steady-state water flux increased with applied potential over the entire potential region 0.025−1 V; the water flux increased with applied potential *even in the current saturation regime*. Returning to Figure 2, in hours 6−8 and 8−10, after an increase in the applied potential, the water flux increased with time while the current decreased and R_{MEA} increased. *The redistribution of water in the membrane affected the current and water flux in opposite directions* (this might be thought of as negative electro-osmotic drag!). Figure 2 shows that after a step change in the applied potential, there can be an instantaneous increase in the current above its steady-state current saturation value, but the current eventually returns to the saturation value.

Current and water flux as functions of applied potential are shown in Figure 5 for co-current flux at 37, 50, and 70 °C and fixed anode feed RH of 30%. The current density and R_{MEA} showed weak temperature dependencies in both the ohmic and

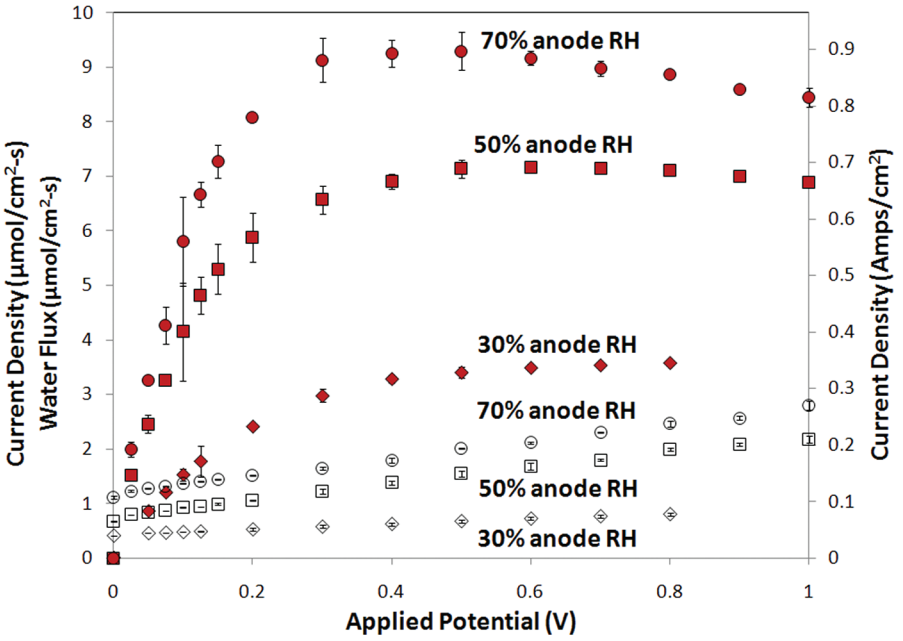

Figure 4. Steady-state current density (filled markers) and water flux (unfilled markers) at different anode feed relative humidities, as a function of applied potential, for co-current flux. All tests were conducted at a temperature of 50 °C. Standard deviations above the marker size of 0.013 A/cm^2 [0.135 μmol/(cm^2 s)] are shown.

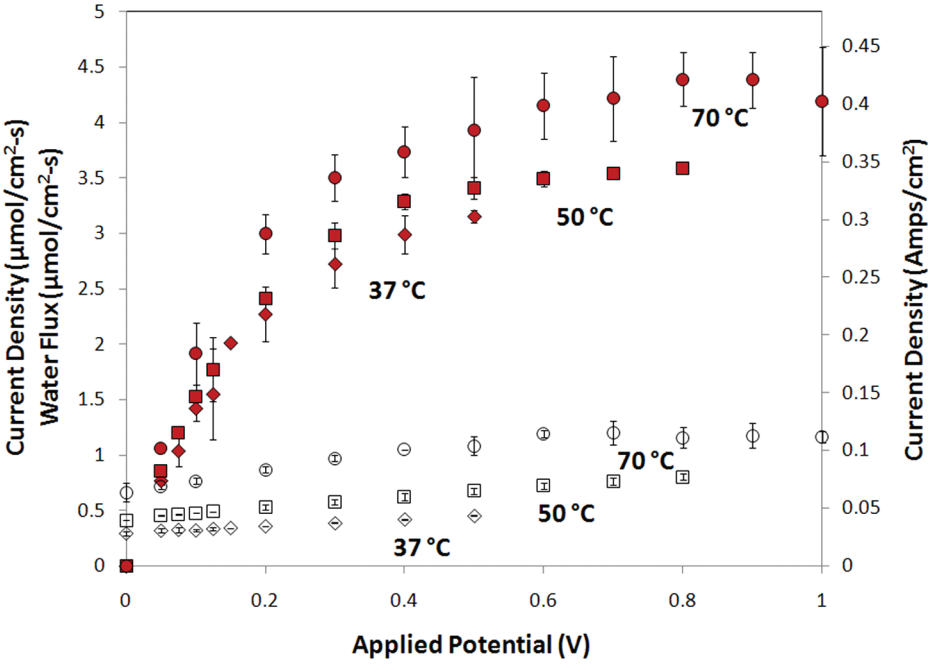

Figure 5. Steady-state current density (filled markers) and water flux (unfilled markers) at different temperatures, as a function of applied potential, for co-current flux. All tests were conducted with humidified hydrogen at an anode feedwater activity of 0.3. Standard deviations above the marker size of 0.01 A/cm^2 [0.104 μmol/(cm^2 s)] are shown.

the saturation regimes. In contrast, there was an increase of the water flux with increasing temperature.

Counter-Current Flux: Current, MEA Resistance, and Water Flux Measurements. In counter-current flux, humidified nitrogen was supplied to the cathode while dry hydrogen was supplied to the anode of the MEA. Water flux was from the cathode to the anode, opposite to the direction of any proton current. At open circuit (i.e., J = 0 A/cm^2) and the same feedwater activity (i.e., either 50% cathode feed RH or 50% anode feed RH), the water flux was the same for counter-current and co-current flux configurations, though in opposing directions. Also, the open circuit voltage of 0.10 V was the same for both counter-current and co-current flux configurations. Unexpectedly, R_{MEA} at open circuit was a factor of 3 larger for the

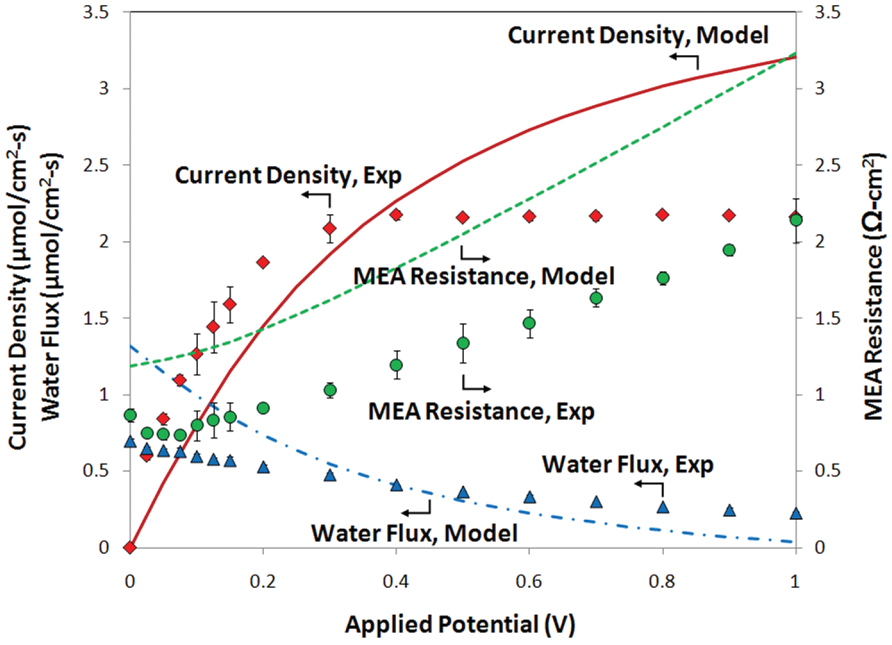

Figure 6. Steady-state current density, water flux, and R_{MEA} as functions of applied potential for counter-current flux at 50 °C, 50% RH cathode feed. Standard deviations above the marker size are shown: 0.002 A/cm^2 [0.021 μmol/(cm^2 s)] for the current density, 0.015 μmol/(cm^2 s) for the water flux, and 0.04 Ω cm^2 for R_{MEA}. The solid and dashed lines are the results of solving the linear transport model, which will be described in the Discussion. Parameters for the model are listed in Table 4.

counter-current flux configuration than the co-current flux configuration. Even though the water activity gradient, the water flux and the open circuit voltage (OCV) were the same for co-current and counter-current flux configurations, the MEA resistances were different. Potential causes for these results will be discussed later.

Application of a potential resulted in a proton current from the anode to the cathode in the opposite direction of the external vapor phase water partial pressure gradient ($p_{w,g}^{anode} < p_{w,g}^{cathode}$). This flux configuration mimics PEM fuel cells that typically have the external water gradient from cathode to anode counter to the direction of the current. Figure 6 summarizes the steady-state current, water flux, and MEA resistance at 50 °C as a function of applied potential with cathode feed of 50% RH N_2 and dry H_2 anode feed. The complete steady-state data set and model calculations for Figure 6 are archived as Supporting Information. As was seen with the co-current flux configuration, the current initially increased linearly with applied potential up to 0.3 V and then saturated; however, the saturation current was reduced by a factor of 3 for counter-current flux compared to co-current flux. This difference in current is consistent with the larger R_{MEA} observed with the counter-current flux configuration. The counter-current water flux decreased with increasing applied potential. The MEA resistance increased with increasing applied potential. Figure 6 also shows the results of solving the linear transport model which will be described in the Discussion.

No-Current: Water Flux and MEA Resistance Measurements. The water flux measurements from both co-current and counter-current flux configurations showed continuous changes in water flux with increasing applied potential, even after the current saturated. In the no-current configuration, water flux was measured using humidified nitrogen supplied to the "anode" while dry nitrogen was supplied to the "cathode". When $V_{app} < 1$ V, there was no protonic current, no change in R_{MEA} and no change in water flux. R_{MEA} and the water flux were the same as those observed for counter-current flow at open circuit. R_{MEA} was lower for the co-current flux configuration at open circuit; i.e., the resistance was reduced when the humidified gas stream was hydrogen instead of nitrogen. Possible explanations for the effect of gas composition on R_{MEA} will be discussed later.

DISCUSSION

The dynamic data from our experiments show that current density, MEA resistance (R_{MEA}), and water flux respond to changes in applied potential with a time constant of ~3000 s at 50 °C. Step changes of applied potential initially cause a sudden increase in water flux and current, but subsequently the current decreases and water flux increases to the steady-state values. The dynamic changes of water flux due to an applied potential were only seen when there was a protonic current. We assert that the coupling of electro-osmotic drag, water diffusion, and interfacial water transport resulted in the redistribution of water in the membrane. The redistribution of water is associated with water desorption from one part of the membrane and water sorption into another part of the membrane. As shown by Satterfield and Benziger,[18] the kinetics of water sorption at 30−50 °C has time constants of 3000−5000 s, comparable to the dynamic changes in current, R_{MEA}, and water flux observed in the experiments reported here.

The key experimental observations from the steady-state experimental data are

1. Current density saturates with increasing applied potential. Current increases linearly with applied potential up to 0.3 V (ohmic regime) and then saturates for applied potentials >0.3 V (saturation regime).
2. The water flux increases in the direction of current flow with applied potential. Even when the steady-state current saturated, the water flux increases with applied potential.

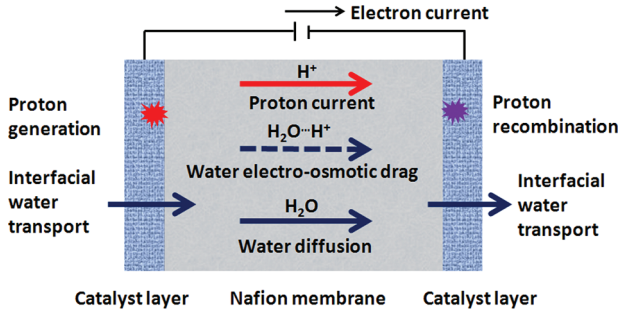

Figure 7. Schematic of co-current flux transport processes for protons and water.

3. R_{MEA} increases with applied potential when there is a protonic current.

Water transport in PEMs has typically assumed a linear superposition of water diffusion and electro-osmotic drag given by eq 3.

$$\text{water flux} = c_w D_w \frac{da_w}{dx} + \xi J \tag{3}$$

Most models of water transport have solved eq 3 by assuming that water activity at the membrane surfaces are at equilibrium with the contacting fluid phase. Recent studies of water transport across Nafion membranes have shown that water activity at the membrane surface may not be at equilibrium with the contacting vapor. Interfacial transport resistances were found to significantly limit the transport of water across the membrane/vapor interface.[13,14,19−21] Interfacial transport resistances might then be expected to affect the net water transport from electro-osmotic drag. We present here a linearized steady-state model of water and proton transport that includes interfacial transport, diffusion, and electro-osmotic drag (EOD).

Water and Proton Transport in PEM Membranes. Figure 7 highlights the transport processes for water and protons across a membrane-electrode assembly. Interfacial water transport, water diffusion, electro-osmotic drag, and proton transport are coupled because the driving forces for all these transport processes are functions of the local water activity. Any change in the distribution of water across the membrane will alter both water and proton transport.

Equations 4−7 describe the steady-state fluxes of water and protons across the membrane. Water transport across the membrane/vapor interfaces at the anode and cathode is given by an interfacial transport coefficient, k_i, multiplied by the water activity difference across the interface. The water activity in the gas phase is defined as the partial pressure of water divided by the vapor pressure of water ($a_{w,g} = P_w/P_w^\circ$). For an ideal solution, the water activity in the membrane is the ratio of water concentration in the membrane to the water concentration in a membrane equilibrated with saturated vapor ($a_{w,m} = c_{w,m}/c_{w,m}$ ($@P_w = P_w^\circ$)). For simplicity, we assumed that k_i is only a function of temperature, and as such, is the same at the anode and cathode gas/membrane interface. We have not tried to separate different components of the interfacial transport resistance for water. There will be resistances associated with the phase change at the membrane/vapor interface, the gas phase diffusional resistance across the gas diffusion layer, and a gas phase boundary layer at the GDL surface in the gas plenum. On the basis of the results of Majsztrik et al.,[13] we believe that the interfacial resistance due to phase change is dominant in our experiments.

Water transport in the membrane is assumed to be the sum of (i) diffusion driven by the water activity gradient and (ii) electro-osmotic drag driven by the current. k_m is the internal transport coefficient for diffusion across the membrane ($k_m = c_w(D_w/t_m)$, where c_w is concentration of water in mol/cm^3, D_w is the diffusivity of water in cm^2/s, and t_m is the thickness of the membrane in cm), ξ_m is the intrinsic electro-osmotic drag coefficient for water internal to the membrane, and J is the current density. a_w represents water activity; the subscripts and superscripts represent location (anode or cathode side, and in the membrane (m) or in the vapor (g) phase). The proton flux or current density is the ratio of the potential drop across the membrane, V_m, to the areal resistance of the membrane, R_m. The transport coefficients, k_m, ξ_m, and R_m, are assumed to be constant averaged values that are, in general, functions of the water activities in the membrane at the membrane/anode and membrane/cathode interfaces.

Anode Gas/Membrane Interface

$$\text{water flux} = k_i(a_{w,g}^{\text{anode}} - a_{w,m}^{\text{anode}}) \tag{4}$$

Membrane

$$\text{water flux} = c_w \frac{D_w}{t_m}(a_{w,m}^{\text{anode}} - a_{w,m}^{\text{cathode}}) + \xi_m J$$

$$= k_m(a_{w,m}^{\text{anode}} - a_{w,m}^{\text{cathode}}) + \xi_m J \tag{5}$$

$$\text{proton flux} = J = \frac{V_m}{R_m} \tag{6}$$

Cathode Membrane/Gas Interface

$$\text{water flux} = k_i(a_{w,m}^{\text{cathode}} - a_{w,g}^{\text{cathode}}) \tag{7}$$

The direct observable quantities are the gas phase water activities at the anode and cathode, and the current density. The steady-state water fluxes must be the same at the interfaces and in the membrane; eqs 4, 5, and 7 may be combined to eliminate the water activities inside the membrane and give the water flux as a function of the transport coefficients and the observable driving forces for water transport, i.e., the difference in vapor phase water activity between the anode and cathode, and the current density.

The water flux, given by eq 8, is the sum of two terms: water transport by diffusion and electro-osmotic drag. Both flux contributions are reduced by a factor that includes the ratio of the diffusion transport coefficient, k_m to the interfacial transport coefficient, k_i. If there were no interfacial transport resistance, $k_i \to \infty$, eq 8 reduces to eq 3. Interfacial transport resistance reduces the impact of both diffusional transport and electro-osmotic drag of water on water flux.

$$\text{water flux} = \text{water activity driven water transport} + \text{net EODwater flux} = \frac{k_m(a_{w,g}^{\text{anode}} - a_{w,g}^{\text{cathode}})}{1 + 2k_m/k_i} + \frac{\xi_m J}{1 + 2k_m/k_i} \tag{8}$$

Table 3. Steady-State Transport: Net Electro-osmotic Drag Coefficient

configuration	J_{sat} (A/cm^2)	water flux [μmol/(cm^2 s)]	k_i [μmol/(cm^2 s)]	k_m [μmol/(cm^2 s)]	$\xi_{net}/\xi_m = 1/(1 + 2k_m/k_i)$	ξ_{net} = Δwater flux/(J/F)
co-current flux 30% RH, 37 °C	0.304	0.454	4.82×10^{-6}	5.23×10^{-6}	0.315	0.051
co-current flux 30% RH, 50 °C	0.346	0.801	6.75×10^{-6}	7.13×10^{-6}	0.321	0.108
co-current flux 30% RH, 70 °C	0.405	1.164	1.15×10^{-5}	9.93×10^{-6}	0.366	0.119
co-current flux 50% RH, 50 °C	0.664	2.179	6.75×10^{-6}	2.80×10^{-5}	0.108	0.219
co-current flux 70% RH, 50 °C	0.815	2.804	6.75×10^{-6}	5.39×10^{-5}	0.059	0.170
counter-current flux 50% RH, 50 °C	0.209	0.226	6.75×10^{-6}	2.20×10^{-5}	0.133	0.217

Electro-osmotic Drag Coefficient. The net electro-osmotic drag coefficient (ξ_{net}) is the change in water flux due to the applied potential divided by the current density as given by eq 9. Net electro-osmotic drag coefficients, ξ_{net}, are reduced from electro-osmotic drag within the membrane, ξ_m, as a result of the interfacial transport resistance, k_i.

$$\xi_{net} = \frac{(\text{water flux@}V_{app} > 0) - (\text{water flux@}V_{app} = 0)}{J} = \frac{\xi_m}{1 + 2k_m/k_i} \quad (9)$$

Net electro-osmotic drag coefficients, ξ_{net}, were calculated for the different flux configurations and are summarized in Table 3. ξ_{net} ranges from 0.05 to 0.22, which are among the lower values reported in the literature. Low values of ξ_{net} may in part be due to the low water activities tested, but we suggest that the major contributor to the low values is interfacial transport resistance.

Majsztrik et al.[13] and Zhao et al.[14] recently measured water liquid and vapor transport coefficients for Nafion. Table 3 summarizes k_m, k_i, and the ratio of ξ_{net} to ξ_m for the experimental conditions of the present study. The values in Table 3 suggest that ξ_{net} is substantially reduced compared to ξ_m when there is only water vapor present at the membrane interface.

According to eq 9, $\xi_{net} \rightarrow \xi_m$ when k_i becomes large, i.e., when there is negligible interfacial resistance for water transport. Majsztrik et al. and Zhao et al. showed that interfacial water transport is nearly equilibrated at the liquid water/membrane interface. Experiments with liquid water present at both sides of the membrane should measure net electro-osmotic drag coefficients values that are close to ξ_m. Zawodzinski et al. carried out such an experiment and measured ξ between 2 and 2.9;[22] this is among the larger values of ξ reported and one we suggest is most representative of ξ_m. In another paper, Zawodzinski and co-workers reported lower ξ values with saturated vapor than with saturated liquid.[23] We submit that the lower ξ values reported for vapor equilibrated membrane are due to the interfacial transport resistance. Experiments conducted with one or both sides of the membrane exposed to water vapor (instead of liquid water) will determine ξ_{net}, and not ξ_m.

How does temperature affect ξ_{net}? A model for vapor/membrane interfacial transport was developed by Monroe et al.;[19] it predicted that k_i should increase proportionally to the vapor pressure of water. That prediction is consistent with the experimental values of k_i determined by Majsztrik et al.[13] Zhao et al.[14] showed that the internal transport coefficient for diffusion in Nafion, $k_m \approx c_w D_m/t_m$, increases more slowly with temperature than k_i. Therefore, we predict that for the same feedwater activity, ξ_{net} should increase with increasing temperature. The experimental data presented in Table 3 shows an increase in ξ_{net} with increasing temperature.

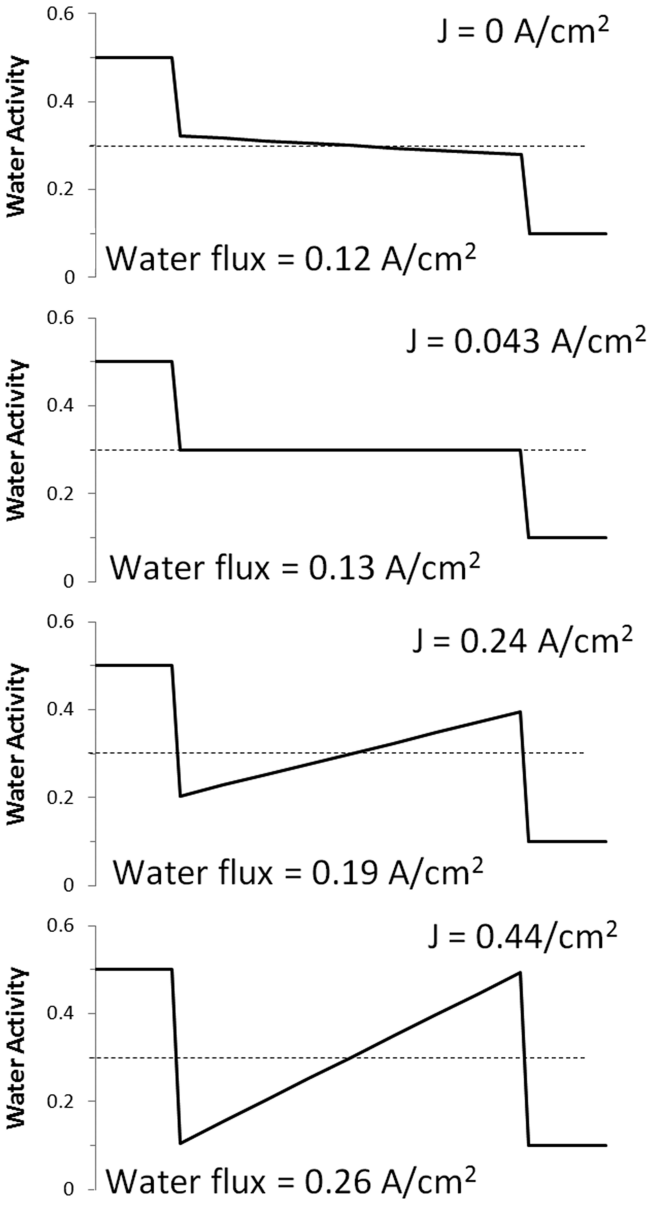

Figure 8. Evolution of the water activity profile in the membrane for co-current flux as a function of current density, based on the linear model. Parameters for the model are listed in Table 4.

It is difficult to attempt to rescale all the ξ values reported in the literature because experimental details are not always fully

documented. However, the general trend of the studies summarized in Table 1 shows that the studies involving liquid water report larger ξ values. Studies with vapor equilibrated membranes report reduced ξ values and these ξ values are larger when the temperature is higher. We suggest that many of the differences in reported values of ξ may be the result of neglecting the interfacial transport resistance at the membrane/vapor interface.

Effect of the Applied Potential on Current, Water Flux, and R_{MEA}. The coupling of interfacial water transport with electro-osmotic drag causes the water to redistribute across the membrane. Figure 8 shows a sequence of water activity profiles and the water flux across an MEA for increasing current density for co-current flux operation assuming constant values of k_m, k_i, and ξ_m. The water activity profiles and water flux were calculated from eqs 4−7 with fixed gas phase water activity at the anode and cathode. Averaged values of k_m were evaluated assuming a linear water activity profile in the membrane.

The membrane water activity decreased from anode to cathode at open circuit (i.e., $J = 0$ A/cm^2). As the current density increases, the water activity profile flipped and the water activity in the membrane increased from the anode to the cathode. Electro-osmotic drag removes water from the anode side of the membrane and interfacial transport limits restocking of water into the membrane, thus causing water activity at the anode to decrease.

The water profiles shown in Figure 8 assumed that the current density could be set arbitrarily. However, the current density is not an independent parameter; it is dependent on the applied potential and the membrane resistance. A decrease in membrane water activity causes the membrane resistance to increase, thus limiting the current and in turn, the electro-osmotic drag.

The areal membrane resistance, R_m, is given by the integral of the local resistivity across the membrane as shown by eq 10.

$$R_m = \int_0^{t_m} \rho_m(a_w(x))\, dx \tag{10}$$

Membrane resistivity, ρ_m, as a function of water activity is well approximated by $\rho_m = \rho_0/a_w{}^2$ (Ω cm). Assuming a linear water activity gradient in the membrane (as shown in Figure 8), with $a_{w,m}^{anode}$ and $a_{w,m}^{cathode}$ as the water activities in the membrane at the respective interfaces, the areal membrane resistance is given by eq 11.

$$R_m = \rho_0 t_m / a_{w,m}^{anode} a_{w,m}^{cathode} \tag{11}$$

To explicitly include the effect of applied voltage on the water and the proton fluxes, eqs 6 and 11 were combined with eq 8 to give the expression for the water flux shown in eq 12:

$$\text{water flux} = \frac{k_m(a_{w,g}^{anode} - a_{w,g}^{cathode}) + \dfrac{\xi_m V_m a_{w,m}^{anode} a_{w,m}^{cathode}}{\rho_0 t_m}}{1 + 2k_m/k_i} \tag{12}$$

The linear transport model was solved as a function of applied potential; the values of the parameters k_i, k_m, ρ_0, and ξ_m were estimated from literature and listed in Table 4. t_m is 0.0127 cm for the Nafion 115 membrane.

The model is compared to the experimental data in Figure 3 for the co-current flux configuration. The model is semiquantitative, capturing the essential experimental trends with increasing applied potential: (i) the water flux increased; (ii) the current density initially increased linearly, followed by saturation at higher applied potentials; (iii) the MEA resistance first decreased and then increased. The fit to the data is remarkable as the only adjustable parameter introduced was the intrinsic electro-osmotic drag coefficient; the other parameters were from independent water uptake and transport experiments. The model did assume averaged parameter values based on linear water activity profiles; relaxation of that assumption would improve the quantitative fit to the data.

Table 4. Model Parameter Values

parameter	values
specific resistivity, ρ_0	7.0 Ω cm
membrane thickness, t_m	0.0127 cm
interfacial transport coefficient, k_i	6.75 μmol/(cm^2 s)
intrinsic electro-osmotic drag coefficient, ξ_m	3
co-current flux configuration:	
water activity of the anode vapor phase, $a_{w,g}^{anode}$	0.5
water activity of the cathode vapor phase, $a_{w,g}^{cathode}$	0.1
internal transport coefficient for diffusion, k_m	28.0 μmol/(cm^2 s)
counter-current flux configuration:	
water activity of the anode vapor phase, $a_{w,g}^{anode}$	0.05
water activity of the cathode vapor phase, $a_{w,g}^{cathode}$	0.5
internal transport coefficient for diffusion, k_m	22.0 μmol/(cm^2 s)

The minimum in the MEA resistance coincides with the water activity becoming uniform within the membrane. The water activity profile in the membrane changes with increasing applied potential due to the redistribution of water. Figure 9 shows the change in the water activity as functions of the applied potential, both in the vapor and in the membrane, at the anode and cathode sides of the membrane. Coupling of EOD and interfacial water transport causes the membrane water activity to decrease at the anode and increase at the cathode. The current density and water flux both saturate and the membrane water activity approaches a limiting value. As EOD depletes water from the anode side of the membrane, the local membrane resistivity increases rapidly and the overall MEA resistance increases superlinearly, as shown in Figure 9.

The large increase in resistance limits the current density; the membrane is self-regulating. If EOD starts to dry out the membrane, then the membrane resistance increases, limiting the current, keeping the membrane from further drying out. Figure 9 shows how the water activity at the anode side of the membrane approaches a limiting value of $a_{w,m}^{anode} \rightarrow 0.1$ with increasing applied potential. Experimentally, this self-regulation is seen in Figure 2 at hours 8−10. The increase in applied potential caused the current to increase, which led to a redistribution of the water in the membrane that increased the membrane resistance. As the membrane resistance increased, the current decrease to its steady-state value. At steady state, the interfacial transport of water into the membrane at the anode is balanced by the electro-osmotic drag of water away from the anode and the back-diffusion of water from the cathode to the anode (because the water activity is increasing from the anode to the cathode; refer to Figure 8 for $J > 0.043$ A/cm^2).

Figures 8 and 9 highlight how electro-osmotic drag causes a redistribution of water in the membrane. Even though the external water activities at the anode and cathode may be fixed, the water activity gradient internal to the membrane may be in

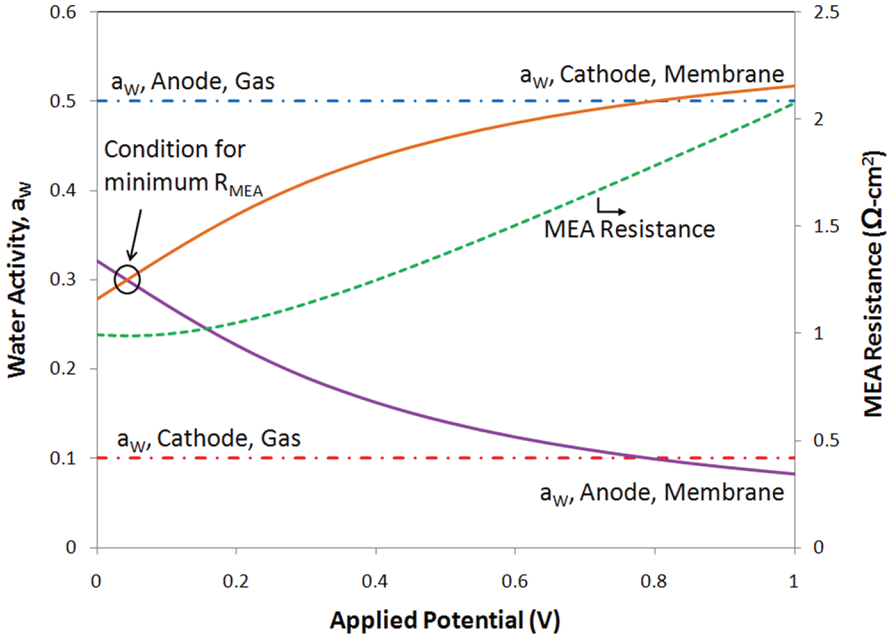

Figure 9. Water activity in the gas phase and in the membrane, at the anode and cathode vapor/membrane interfaces, for co-current flux as a function of applied potential, based on the linear model. The overall areal membrane resistance increases as the membrane water activity at the anode decreases. Parameters for the model are listed in Table 4.

the reverse direction. This is a key point about the coupling of interfacial transport resistance and electro-osmotic drag: the water activities at the membrane interfaces may be enriched or depleted relative to the water activity in the contacting vapor phase. With the exception of having liquid water at both sides of the MEA, it is impossible to fix the membrane water activity at a constant value to study electro-osmotic drag.

In the analysis presented above, it was assumed that ξ_m is constant. However, ξ_m could be a function of water activity. The variation of ξ_m with water activity could accentuate or reduce the water activity gradients internal to the membrane. However, it appears that there is no easy way to separate the effects of EOD and interfacial water transport.

The linear transport model was also solved for the counter-current flux configuration. The model is compared to the experimental data in Figure 6. The model again captures the essential experimental trends with increasing applied potential: (i) the water flux decreased; (ii) the current density initially increased linearly, followed by saturation at higher applied potentials; (iii) the MEA resistance increased.

Deficiencies of the Model. The simplified linear model presented does a remarkable job reproducing the experimental observations for both co-current and counter-current flux configurations. Two experimental observations were not captured by the linear model: (i) the experimental data showed the water flux increased after the current had saturated; the model predicted they should saturate together; (ii) the model did not account for a difference in the membrane resistance when the humidified gas was nitrogen instead of hydrogen.

We suspect the increase in water flux with increased applied potential in the current saturation regime was caused by different nonlinear dependencies of water diffusivity and proton conduction. Water diffusion coefficients increase as $(a_w)^2$ and the membrane resistance increases as $(a_w)^{-1}$. We also suspect that ξ_m may also change with water activity (the existing data is not definitive of this). The model could be adjusted to fit the data by introducing nonlinear transport coefficients and a water activity dependent EOD coefficient; we have not pursued that here because of the ad-hoc nature of the adjustable parameters with a nonlinear model.

The experimental data showed that the membrane resistance was greater and the current density lower when the humidified gas stream was nitrogen compared to when the humidified gas stream was hydrogen. We believe this resulted from the dependence of the interfacial transport coefficients on the gas phase composition. With a porous electrode, the interfacial transport coefficients will depend on the gas phase diffusion coefficient. The diffusivity of water in H_2 is greater than diffusivity of water in N_2, $D_{w,H_2} > D_{w,N_2}$. When the humidified gas stream is nitrogen, the smaller k_i will reduce the rate of water transport into the membrane, thus reducing the water activity at the anode membrane interface and increasing the membrane resistance. The model could be modified to include different k_i's at the two interfaces, but this again is beyond the scope of this paper.

Implications for Fuel Cell Operation. The coupling of the membrane resistance to EOD in a fuel cell is self-regulating. Interfacial water transport limits the restocking of water into the membrane, while EOD reduces the water activity at the anode, thus increasing the membrane resistance. Increasing the membrane resistance limits the current, thus reducing electro-osmotic drag and keeping the membrane from drying out. EOD has a minor adverse effect on fuel cell operation; it will reduce the maximum current density. But the self-regulation of the membrane resistance will prevent the often suggested catastrophic failure. The impact of EOD on PEM fuel cell performance has been, in our opinion, overestimated because the effect of interfacial transport resistance at the membrane/vapor interface on water transport has not been appropriately considered.

The self-regulation of current density via the membrane resistance also has an important implication for fuel cell sizing

and control. The dynamic data showed that in the current saturation regime, when there was a step change in potential, the current can peak at almost 1.5 times its saturation value for ~100 s. Fuel cell sizing is often based on peak power. But if the peak power is only required intermittently for short periods of time (e.g., during engine acceleration), it may be possible to employ smaller fuel cells whose size is based on the steady-state requirements.

CONCLUSIONS

The present study showed that interfacial water transport plays a dominant role in the coupling of water and proton transport in Nafion. The key results are

1. The dynamic changes in current, water flux, and MEA resistance to step changes in applied potential, with a time constant of ~3000 s, strongly suggest that water redistributes in the membrane due to the coupling of interfacial water transport in and out of the Nafion membrane, and electro-osmotic drag (EOD) inside the membrane.
2. Interfacial water transport resistance limits the rate at which water can enter or leave Nafion membranes. Both water diffusion and electro-osmotic drag in the membrane are reduced by the ratio of the diffusion transport coefficient to the interfacial transport coefficient.
3. The net EOD is less than the intrinsic EOD internal to the Nafion membrane because of interfacial transport resistance at the vapor/membrane interface. The difference between ξ_{net} and ξ_m is minimized with liquid equilibrated membranes.
4. EOD affects the water activity profile in the membrane, which in turn affects proton transport and water transport because both these transport processes are dependent on water activity.
5. At low applied potentials, the protonic current increased with potential. For larger applied potentials, the current saturated. The saturation current increased with increased feedwater activity. The saturation current is controlled by a balance of interfacial water transport across the membrane/vapor interface, diffusion to the interface, and electro-osmotic drag away from the interface.
6. Interfacial transport resistance at the vapor/membrane interface retains water in Nafion membranes in fuel cells, thus reducing the effect of electro-osmotic drag on overall water flux.
7. Feedback coupling between electro-osmotic drag and membrane resistance self-regulates the current in PEM fuel cells.

ASSOCIATED CONTENT

Supporting Information. The complete data sets for (i) the dynamic data presented in Figure 2, (ii) the co-current steady state-data presented in Figure 3, and (iii) the counter-current steady-state data presented in Figure 6, are available as Excel files. This material is available free of charge via the Internet at http://pubs.acs.org.

AUTHOR INFORMATION

Corresponding Author

*Phone: (609) 258-5416. Fax: (609) 258-0211. E-mail: benziger@princeton.edu.

ACKNOWLEDGMENT

We thank the National Science Foundation (CBET-0754715) and Department of Energy (DE-SC-0002097) for partial support of this work. M.J.C. also thanks the Princeton University Program in Plasma Science and Technology for partial support under U.S. Department of Energy contract No. DE-AC02-76-CHO-3073.

REFERENCES

(1) Eikerling, M.; Kharkats, Y. I.; Kornyshev, A. A.; Volfkovich, Y. M. *J. Electrochem. Soc.* **1998**, *145*, 2684.
(2) Buchi, F. N.; Scherer, G. G. *J. Electrochem. Soc.* **2001**, *148*, A183.
(3) Buchi, F. N.; Srinivasan, S. *J. Electrochem. Soc.* **1997**, *144*, 2767.
(4) Williams, M. V.; Kunz, H. R.; Fenton, J. M. *J. Power Sources* **2004**, *135*, 122.
(5) Siegel, J. B.; McKay, D. A.; Stefanopoulou, A. G.; Hussey, D. S.; Jacobson, D. L. *J. Electrochem. Soc.* **2008**, *155*, B1168.
(6) Dhar, H. P. *J. Power Sources* **2005**, *143*, 185.
(7) Hogarth, W. H. J.; Benziger, J. B. *J. Power Sources* **2006**, *159*, 968.
(8) Kreuer, K. D. *Chem. Mater.* **1996**, *8*, 610.
(9) Elliott, J. A.; Paddison, S. J. *Phys. Chem. Chem. Phys.* **2007**, *9*, 2602.
(10) Eikerling, M.; Kornyshev, A. A.; Kuznetsov, A. M.; Ulstrup, J.; Walbran, S. *J. Phys. Chem. B* **2001**, *105*, 3646.
(11) Choi, P.; Jalani, N. H.; Datta, R. *J. Electrochem. Soc.* **2005**, *152*, E123.
(12) Pivovar, B. S. *Polymer* **2006**, *47*, 4194.
(13) Majsztrik, P.; Bocarsly, A.; Benziger, J. *J. Phys. Chem. B* **2008**, *112*, 16280.
(14) Zhao, Q. A.; Majsztrik, P.; Benziger, J. *J. Phys. Chem. B* **2011**, *115*, 2717.
(15) Majsztrik, P. W.; Satterfield, M. B.; Bocarsly, A. B.; Benziger, J. B. *J. Membr. Sci.* **2007**, *301*, 93.
(16) Rohland, B.; Eberle, K.; Strobel, R.; Scholta, J.; Garche, J. *Electrochim. Acta* **1998**, *43*, 3841.
(17) Casati, C.; Longhi, P.; Zanderighi, L.; Bianchi, F. *J. Power Sources* **2008**, *180*, 103.
(18) Satterfield, M. B.; Benziger, J. B. *J. Phys. Chem. B* **2008**, *112*, 3693.
(19) Monroe, C. W.; Romero, T.; Merida, W.; Eikerling, M. *J. Membr. Sci.* **2008**, *324*, 1.
(20) Adachi, M.; Navessin, T.; Xie, Z.; Li, F. H.; Tanaka, S.; Holdcroft, S. *J. Membr. Sci.* **2010**, *364*, 183.
(21) Kientiz, B.; Yamada, H.; Nonoyama, N.; Weber, A. Z. *J. Fuel Cell Sci. Technol.* **2011**, *8*, 011013.
(22) Zawodzinski, T. A.; Springer, T. E.; Davey, J.; Jestel, R.; Lopez, C.; Valerio, J.; Gottesfeld, S. *J. Electrochem. Soc.* **1993**, *140*, 1981.
(23) Zawodzinski, T. A.; Davey, J.; Valerio, J.; Gottesfeld, S. *Electrochim. Acta* **1995**, *40*, 297.
(24) Fuller, T. F.; Newman, J. *J. Electrochem. Soc.* **1992**, *139*, 1332.
(25) Gallagher, K. G.; Pivovar, B. S.; Fuller, T. F. *J. Electrochem. Soc.* **2009**, *156*, B330.
(26) Xie, G.; Okada, T. *J. Electrochem. Soc.* **1995**, *142*, 3057.
(27) Ise, M.; Kreuer, K. D.; Maier, J. *Solid State Ion.* **1999**, *125*, 213.
(28) Ren, X. M.; Gottesfeld, S. *J. Electrochem. Soc.* **2001**, *148*, A87.
(29) Park, Y. H.; Caton, J. A. *Int. J. Hydrog. Energy* **2008**, *33*, 7513.
(30) Weng, D.; Wainright, J. S.; Landau, U.; Savinell, R. F. *J. Electrochem. Soc.* **1996**, *143*, 1260.
(31) Ge, S. H.; Yi, B. L.; Ming, P. W. *J. Electrochem. Soc.* **2006**, *153*, A1443.
(32) Ye, X. H.; Wang, C. Y. *J. Electrochem. Soc.* **2007**, *154*, B676.
(33) Luo, Z. P.; Chang, Z. Y.; Zhang, Y. X.; Liu, Z.; Li, J. *Int. J. Hydrogen Energy* **2010**, *35*, 3120.